Advanced Composite Materials
Publication details, including instructions for authors and subscription information:
http://www.tandfonline.com/loi/tacm20

Stress analysis of laminated composite annular disks subjected to a concentrated transverse load using layer-wise zig-zag theory

Deoggyu Lee [a] & Anthony M. Waas [b]

[a] Composite Structures Laboratory, Department of Aerospace EngiaZeering, The University of Michigan, Ann Arbor, MI 48109-2118, USA

[b] Composite Structures Laboratory, Department of Aerospace EngiaZeering, The University of Michigan, Ann Arbor, MI 48109-2118, USA

Version of record first published: 02 Apr 2012.

To cite this article: Deoggyu Lee & Anthony M. Waas (1997): Stress analysis of laminated composite annular disks subjected to a concentrated transverse load using layer-wise zig-zag theory, Advanced Composite Materials, 6:4, 261-277

To link to this article: http://dx.doi.org/10.1163/156855197X00139

Adv. Composite Mater., Vol. 6, No. 4, pp. 261–278 (1997)

Stress analysis of laminated composite annular disks subjected to a concentrated transverse load using layer-wise zig-zag theory

DEOGGYU LEE* and ANTHONY M. WAAS**

Composite Structures Laboratory, Department of Aerospace Engineering, The University of Michigan, Ann Arbor, MI 48109-2118, USA

Received 15 July 1996; accepted 26 September 1996

Abstract—This paper presents accurate inter-lamina stress distributions of laminated composite annular disks incorporating layer-wise zig-zag theory. This theory is based on the superposition of a global higher order shear deformation displacement field and a local linear zig-zag displacement field (RHOT). RHOT automatically satisfies displacement continuity at the layer interfaces and by further application of stress continuity at the layer interfaces and traction free boundary conditions, the unknown degrees of freedom are reduced to seven regardless of the number of layers. These are two in-plane displacements, two shear rotations, a transverse displacement and two section rotations. A four-node sector finite element in a cylindrical coordinate system is developed using RHOT. Two in-plane displacements and two shear rotations which are C^0 continuous are interpolated using bilinear functions and a transverse displacement and two section rotations which are C^1 continuous are interpolated using higher order Hermitian functions. In-plane normal stress and inter-lamina transverse shear stress variation through the thickness are calculated for laminated disks using a RHOT sector element and comparison is made with first order shear deformation theory predictions. The present work precedes the application of the zig-zag theory to transient dynamic analysis and is a first step at establishing the accuracy of implementing the zig-zag theory into a sector finite element.

Keywords: Composite disks; stress analysis; finite elements; layer-wise theory.

1. INTRODUCTION

Accurate predictions of inter-lamina transverse shear stress distributions through the thickness of laminated disks is crucial in determining delamination failures in layered disks such as optical recording disks in the information storage industry. Delamination eventually causes damage via non-uniform contact leading to poor recording quality and eventual breakdown.

---

*Doctoral Candidate.

**Associate Professor, author to whom correspondence should be sent.

In modeling layered disks, there are two widely used theories which are categorized into equivalent single layer theory and layer-wise zig-zag theory. In the equivalent single layer theory, on reducing the three-dimensional elasticity problem to a two-dimensional one, the laminate is characterized as an equivalent, homogeneous layer. Therefore, the number of governing equations is not dependent on the number of layers comprising a laminate. A major drawback of the equivalent single layer theories is in determining the three-dimensional stress field at the layer level. In this theory, transverse strain components are continuous across interfaces between dissimilar materials, thus leading to transverse stress components that are discontinuous at the layer interfaces. Lo *et al.* [1] derived a equivalent single-layer plate equation using higher order shear deformation theory and analyzed plate bending. Reddy [2, 3] analyzed stability and free vibration of isotropic, orthotropic and laminated plates according to an equivalent single-layer refined higher order shear deformation theory. Mallikarjuna and Kant [4] analyzed free vibration of symmetrically laminated plate using an equivalent single-layer higher order shear deformation theory in conjunction with the finite element method.

In the layer-wise zig-zag theory, a cubic varying displacement field is superimposed on a zig-zag linearly varying displacement field. The cubic variation accounts for the overall parabolic transverse shear distribution known from single layer theory, while the zig-zag accounts for the strain discontinuities that are required between layers to satisfy stress continuity conditions. This theory has the same number of dependent unknowns as the first-order shear deformation theory and the number of unknowns is independent of the number of layers. The displacement field satisfies continuity between layers. The unknown degrees of freedom in this theory can be reduced by applying transverse shear stress continuity conditions at the interface between layers as well as shear free conditions at the top and bottom surfaces of the layered medium. Thus, an artificial shear correction factor is not needed. Di Sciuva [5] developed a linear layer-wise zig-zag plate theory and applied it to the bending and free vibration problem of multilayered orthotropic plates. Murakami [6] analyzed in-plane response of a laminate utilizing the linear zig-zag theory. Di Sciuva [7] also developed a general multilayered anisotropic shell formulation incorporating the linear zig-zag theory. This same author later developed a rectangular plate element utilizing the higher order zig-zag theory [10]. Cho and Parmerter [9] developed a higher order layer-wise zig-zag plate theory and applied it to the cylindrical bending problem in a plate. Averill [11] developed a beam element using the linear zig-zag theory and applied it to the beam bending and free vibration problem. Averill and Yip [12] developed a beam finite element using the higher order zig-zag theory.

In the present work, a sector element incorporating higher order layer-wise zig-zag theory is developed and applied for calculating the in-plane normal stress and inter-lamina transverse shear stress distribution through the thickness of polar-orthotropic laminated disks. Reduced integration techniques are used for the integration of the constitutive equations to prevent the shear locking phenomenon. The in-plane normal stress and inter-lamina transverse shear stress distribution through the thickness is recovered using the constitutive equations after obtained the mid-plane deformation. Results are presented for the static point loading of a layered disk. The present work

is a pre-cursor to the application of layer-wise zig-zag theory to analyze transient structural dynamic response of rotating layered disks [20].

2. LAYER-WISE ZIG-ZAG THEORY (DISCRETE-LAYER THEORY)

A new sector finite element in a cylindrical coordinate system is developed using the refined layer-wise zig-zag theory. The disk is considered to be composed of N layers of uniform thickness perfectly bonded together, where the thickness and constitutive properties are allowed to vary arbitrarily from layer to layer. The reference surface of the disk is allowed to pass through any arbitrary interface. The layer-wise displacement is assumed to be a superposition of a global cubic function in the z-direction which accounts for the overall parabolic transverse shear distribution known from single layer theory and a local linear function in the z-direction which accounts for the strain discontinuities that are required between layers to satisfy stress continuity conditions. The linear zig-zag theory has a different slope in each layer. The displacement field for the k^{th} layer is as follows:

$$\begin{aligned} u^{(k)}(r,\theta,z,t) &= u_0(r,\theta,t) + zu_1(r,\theta,t) + z^2u_2(r,\theta,t) + z^3u_3(r,\theta,t) \\ &\quad + \sum_{i=1}^{k-1}(z-z_i)\xi_i(r,\theta,t) - \sum_{j=1}^{m}(z-z_j)\xi_j(r,\theta,t), \\ v^{(k)}(r,\theta,z,t) &= v_0(r,\theta,t) + zv_1(r,\theta,t) + z^2v_2(r,\theta,t) + z^3v_3(r,\theta,t) \\ &\quad + \sum_{i=1}^{k-1}(z-z_i)\eta_i(r,\theta,t) - \sum_{j=1}^{m}(z-z_j)\eta_j(r,\theta,t), \\ w^{(k)} &= w_0(r,\theta,t), \end{aligned} \tag{1}$$

where the reference surface lies between the m^{th} and $(m+1)^{th}$ layers (Fig. 1). Here u_0, v_0 are the in-plane displacements, w_0 is the transverse displacement, u_1, v_1 are the shear rotations of layer $m+1$ (the layer above the reference surface) and u_2, v_2, u_3, v_3 are higher order rotations. ξ_i, η_i are slopes in each layer.

We can eliminate the degrees of freedom u_2, v_2, u_3, v_3, ξ_i, η_i in the higher order zig-zag displacement function by exploiting the condition of shear stress continuity at the j^{th} interface where $z = z_j$,

$$\tau_{rz}^{(j)} = \tau_{rz}^{(j+1)}, \qquad \tau_{\theta z}^{(j)} = \tau_{\theta z}^{(j+1)}, \tag{2}$$

and the transverse shear free traction boundary conditions at the top ($z = z_N$) and bottom ($z = z_0$) plate surface;

$$\begin{aligned} \tau_{rz}\big|_{z=z_0} &= 0, \qquad \tau_{\theta z}\big|_{z=z_0} = 0, \\ \tau_{rz}\big|_{z=z_N} &= 0, \qquad \tau_{\theta z}\big|_{z=z_N} = 0. \end{aligned} \tag{3}$$

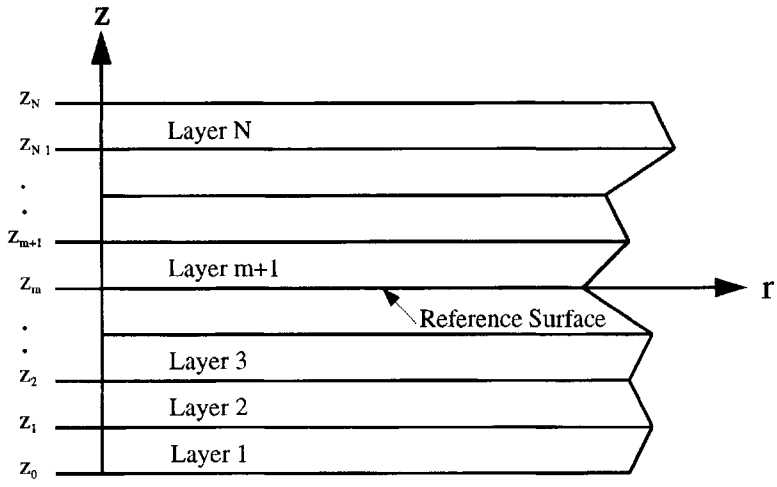

Figure 1. Geometry, coordinates and labeling system used in the present model.

After applying the shear stress continuity conditions and traction free boundary conditions, we obtain refined higher order zig-zag displacement functions which satisfy displacement continuity, shear stress continuity and traction free boundary conditions. These are, for the k^{th} layer;

$$u^{(k)} = u_0 + zu_1 + \left(z^2\beta_1 + z^3\kappa_1 + \left[\sum_{i=1}^{k-1}(z - z_i)a_i^1 - \sum_{j=1}^{m}(z - z_j)a_j^1\right]\right)\left(u_1 + \frac{\partial w_0}{\partial r}\right),$$

$$v^{(k)} = v_0 + zv_1 + \left(z^2\beta_2 + z^3\kappa_2 + \left[\sum_{i=1}^{k-1}(z - z_i)a_i^2 - \sum_{j=1}^{m}(z - z_j)a_j^2\right]\right)\left(v_1 + \frac{1}{r}\frac{\partial w_0}{\partial \theta}\right),$$

$$w^{(k)} = w_0. \tag{4}$$

The coefficients β_i, κ_i, a_i^1, a_i^2, are evaluated as shown in Appendix A.

3. STRAIN ENERGY

The strain energy of the N-layered sectorial area is given by

$$U = \frac{1}{2}\int_{\theta_1}^{\theta_2}\int_{r_1}^{r_2}\left[\sum_{k=1}^{N}\int_{z_{k-1}}^{z_k}\left\{\sigma_r^{(k)}e_r^{(k)} + \sigma_\theta^{(k)}e_\theta^{(k)} + \tau_{r\theta}^{(k)}\gamma_{r\theta}^{(k)} + \tau_{rz}^{(k)}\gamma_{rz}^{(k)} + \tau_{\theta z}^{(k)}\gamma_{\theta z}^{(k)}\right\}\mathrm{d}z\right] r\,\mathrm{d}r\,\mathrm{d}\theta. \tag{5}$$

3.1. Strain-displacement relations

The linear strain-displacement relations for the k^{th} layer in a cylindrical coordinate system are defined as follows:

$$\begin{aligned}
e_r^{(k)} &= \frac{\partial u^{(k)}}{\partial r}, \\
e_\theta^{(k)} &= \frac{1}{r}\frac{\partial v^{(k)}}{\partial \theta} + \frac{u^{(k)}}{r}, \\
\gamma_{r\theta}^{(k)} &= \frac{1}{r}\frac{\partial u^{(k)}}{\partial \theta} + \frac{\partial v^{(k)}}{\partial r} - \frac{v^{(k)}}{r}, \\
\gamma_{\theta z}^{(k)} &= \frac{\partial v^{(k)}}{\partial z} + \frac{1}{r}\frac{\partial w^{(k)}}{\partial \theta}, \\
\gamma_{rz}^{(k)} &= \frac{\partial u^{(k)}}{\partial z} + \frac{\partial w^{(k)}}{\partial r}.
\end{aligned} \tag{6}$$

3.2. Constitutive relation

The linear elastic constitutive relation for any individual layer (k^{th} layer) is given by

$$\begin{Bmatrix} \sigma_r \\ \sigma_\theta \\ \sigma_z \\ \tau_{r\theta} \\ \tau_{rz} \\ \tau_{\theta z} \end{Bmatrix}^{(k)} = \begin{bmatrix} C_{11} & C_{12} & C_{13} & 0 & 0 & 0 \\ C_{12} & C_{22} & C_{23} & 0 & 0 & 0 \\ C_{13} & C_{23} & C_{33} & 0 & 0 & 0 \\ 0 & 0 & 0 & C_{44} & 0 & 0 \\ 0 & 0 & 0 & 0 & C_{55} & 0 \\ 0 & 0 & 0 & 0 & 0 & C_{66} \end{bmatrix}^{(k)} \begin{Bmatrix} e_r \\ e_\theta \\ e_z \\ \gamma_{r\theta} \\ \gamma_{rz} \\ \gamma_{\theta z} \end{Bmatrix}^{(k)} . \tag{7}$$

The reduced stress–strain relation of an orthotropic layer under a plane stress assumption ($\sigma_z = 0$) is

$$\begin{Bmatrix} \sigma_r \\ \sigma_\theta \\ \tau_{r\theta} \\ \tau_{rz} \\ \tau_{\theta z} \end{Bmatrix}^{(k)} = \begin{bmatrix} \bar{C}_{11} & \bar{C}_{12} & 0 & 0 & 0 \\ \bar{C}_{12} & \bar{C}_{22} & 0 & 0 & 0 \\ 0 & 0 & \bar{C}_{44} & 0 & 0 \\ 0 & 0 & 0 & \bar{C}_{55} & 0 \\ 0 & 0 & 0 & 0 & \bar{C}_{66} \end{bmatrix}^{(k)} \begin{Bmatrix} e_r \\ e_\theta \\ \gamma_{r\theta} \\ \gamma_{rz} \\ \gamma_{\theta z} \end{Bmatrix}^{(k)} , \tag{8}$$

where $\bar{C}_{ij} = C_{ij} - \frac{C_{i3}C_{j3}}{C_{33}}$, $i, j = 1, 2, 4$, and $\bar{C}_{ii} = C_{ii}$, $i = 5, 6$.

Explicit relations for $\bar{C}_{ij}$ in terms of engineering constants are given below:

$$\begin{aligned}
\bar{C}_{11} &= \frac{E_1}{(1-\nu_{12}\nu_{21})}, \\
\bar{C}_{12} &= \frac{\nu_{12}E_2}{(1-\nu_{12}\nu_{21})} = \frac{\nu_{21}E_1}{(1-\nu_{12}\nu_{21})}, \\
\bar{C}_{22} &= \frac{E_2}{(1-\nu_{12}\nu_{21})}, \\
\bar{C}_{44} &= G_{12}, \\
\bar{C}_{55} &= G_{31}, \\
\bar{C}_{66} &= G_{23}.
\end{aligned} \tag{9}$$

Here we have adopted the notations in standard texts on lamination theory (for example, Jones [25]).

In addition, the in-plane moduli satisfy the reciprocal relation

$$\frac{\nu_{12}}{E_1} = \frac{\nu_{21}}{E_2}. \tag{10}$$

3.3. *Polar-orthotropy and rectilinear-orthotropy*

Two kinds of orthotropies (polar-orthotropy and rectilinear-orthotropy (see Fig. 2)) are considered in this study. For example, polar-orthotropy in a cylindrical coordinate system can be divided into two categories: in one case, one of the principal material directions is parallel to the radial direction ($\beta = 0°$) and in the other case this direction is parallel to the circumferential direction ($\beta = 90°$). In the case of rectilinear-orthotropy, β assumes angles that are in the range $0° < \beta < 90°$. In this latter case, it is easier to stipulate the principal direction in terms of α, with respect to the Cartesian x-y coordinate system. The above classification becomes quite evident if

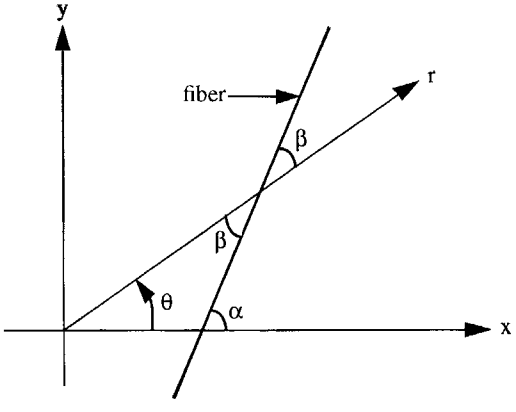

Figure 2. Definition of angles for orthotropy in a cylindrical coordinate system.

one considers a continuous fiber composite lamina. In such a case, the fiber direction is one of the principal material axes for the lamina. Only polar-orthotropic material is considered in the present study.

4. SECTOR FINITE ELEMENT

In this section, a new sector element is derived by use of the refined higher order zig-zag displacement function. This sector element has 7 degrees of freedom (2 in-plane displacements (u_0, v_0), 2 shear rotations (u_1, v_1) and 1 out-of-plane displacement and section rotations (w_0, $\frac{\partial w_0}{\partial r}$, $\frac{\partial w_0}{\partial \theta}$)). So the strategy for the finite element development conforming to the displacement field given by (4) is to use C^0 continuity linear Lagrangian interpolation functions for in-plane displacements and shear rotations and C^1 continuity Hermitian 12-term interpolation functions for the out-of-plane displacement and section rotations. Actually, a sector element in a cylindrical coordinate system is a special case well suited for this hybrid interpolation, quite similar to the rectangular element in a Cartesian coordinate system. Nodal numbering and the degrees of freedom associated with the element are shown in Fig. 3.

The in-plane displacements and shear rotations (C^0) are interpolated using the linear Lagrangian function and a transverse displacement and section rotations (C^1) are interpolated using a Hermitian 12-term function. Thus,

$$\begin{aligned}
u_0 &= a_1 + ra_5 + \theta a_9 + r\theta a_{13},\\
v_0 &= a_2 + ra_6 + \theta a_{10} + r\theta a_{14},\\
u_1 &= a_3 + ra_7 + \theta a_{11} + r\theta a_{15},\\
v_1 &= a_4 + ra_8 + \theta a_{12} + r\theta a_{16},\\
w_0 &= a_{17} + ra_{18} + \theta a_{19} + r^2 a_{20} + r\theta a_{21} + \theta^2 a_{22} + r^3 a_{23}\\
&\quad + r^2\theta a_{24} + r\theta^2 a_{25} + \theta^3 a_{26} + r^3\theta a_{27} + r\theta^3 a_{28}.
\end{aligned} \tag{11}$$

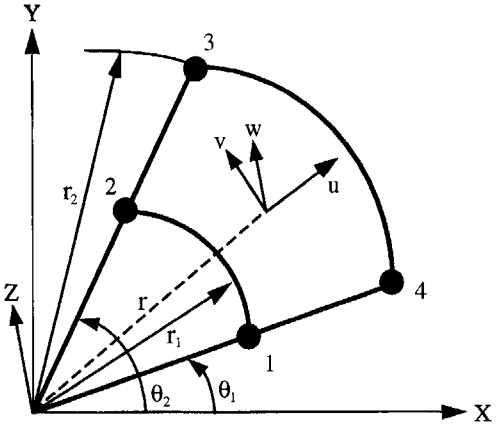

Figure 3. The sector element in cylindrical coordinates.

The 7 degrees of freedom are expressed as:

$$\left\{u_0, v_0, w_0, u_1, v_1, u_1 + \frac{\partial w_0}{\partial r}, v_1 + \frac{1}{r}\frac{\partial w_0}{\partial \theta}\right\}^T = [c]\{a\}. \tag{12}$$

We can extract the equations for the resultant material constants by integration in the thickness direction. Before doing so, the following plate resultants are defined. Membrane and bending stress resultants are defined as

$$\begin{bmatrix} N_r & N_\theta & N_{r\theta} \\ M_r & M_\theta & M_{r\theta} \end{bmatrix} = \sum_{k=1}^{N} \int_{z_{k-1}}^{z_k} \begin{Bmatrix} 1 \\ z \end{Bmatrix} \begin{bmatrix} \sigma_r^{(k)} & \sigma_\theta^{(k)} & \tau_{r\theta}^{(k)} \end{bmatrix} \mathrm{d}z, \tag{13}$$

$$\begin{bmatrix} M_r^{1a} & M_\theta^{1a} & M_{r\theta}^{1a} \end{bmatrix} = \sum_{k=1}^{N} \int_{z_{k-1}}^{z_k} \{z^{1a}\} \begin{bmatrix} \sigma_r^{(k)} & \sigma_\theta^{(k)} & \tau_{r\theta}^{(k)} \end{bmatrix} \mathrm{d}z, \tag{14}$$

$$\begin{bmatrix} M_\theta^{2a} & M_{r\theta}^{2a} \end{bmatrix} = \sum_{k=1}^{N} \int_{z_{k-1}}^{z_k} \{z^{2a}\} \begin{bmatrix} \sigma_\theta^{(k)} & \tau_{r\theta}^{(k)} \end{bmatrix} \mathrm{d}z, \tag{15}$$

where the effective transverse coordinate system in this formulation is defined as:

$$z^{1a} = \sum_{i=1}^{k-1}(z - z_i)a_i^1 - \sum_{j=1}^{m}(z - z_j)a_j^1 + z^2\beta_1 + z^3\kappa_1, \tag{16}$$

$$z^{2a} = \sum_{i=1}^{k-1}(z - z_i)a_i^2 - \sum_{j=1}^{m}(z - z_j)a_j^2 + z^2\beta_2 + z^3\kappa_2, \tag{17}$$

and the shear force resultants are defined as:

$$\begin{bmatrix} Q_r & Q_\theta \end{bmatrix} = \sum_{k=1}^{N} \int_{z_{k-1}}^{z_k} \begin{bmatrix} \tau_{rz}^{(k)} & \tau_{\theta z}^{(k)} \end{bmatrix} \mathrm{d}z, \tag{18}$$

$$\begin{bmatrix} Q_r^{1a} \end{bmatrix} = \sum_{k=1}^{N} \int_{z_{k-1}}^{z_k} \{z^{1aa}\} \begin{bmatrix} \tau_{rz}^{(k)} \end{bmatrix} \mathrm{d}z, \tag{19}$$

$$\begin{bmatrix} Q_\theta^{2a} \end{bmatrix} = \sum_{k=1}^{N} \int_{z_{k-1}}^{z_k} \{z^{2aa}\} \begin{bmatrix} \tau_{\theta z}^{(k)} \end{bmatrix} \mathrm{d}z. \tag{20}$$

The derivatives of the effective transverse coordinate are defined as:

$$z^{1aa} = \sum_{i=1}^{k-1} a_i^1 - \sum_{j=1}^{m} a_j^1 + 2z\beta_1 + 3z^2\kappa_1, \tag{21}$$

$$z^{2aa} = \sum_{i=1}^{k-1} a_i^2 - \sum_{j=1}^{m} a_j^2 + 2z\beta_2 + 3z^2\kappa_2. \tag{22}$$

The force vector and the corresponding kinematic vector are defined as follows. The bending-stretching force vector is

$$\{F\}_b = \left\{N_r, N_\theta, N_{r\theta}, M_r, M_\theta, M_{r\theta}, M_r^{1a}, M_\theta^{1a}, M_{r\theta}^{1a}, M_\theta^{2a}, M_{r\theta}^{2a}\right\}^T, \tag{23}$$

the transverse shear force vector is

$$\{F\}_s = \left\{Q_r, Q_\theta, Q_r^{1a}, Q_\theta^{2a}\right\}^T. \tag{24}$$

The general bending-stretching strain vector is defined as:

$$\begin{aligned}\{X\}_b^L = \Bigg\{ & \frac{\partial u_0}{\partial r}, \frac{1}{r}\frac{\partial v_0}{\partial \theta} + \frac{u_0}{r}, \frac{1}{r}\frac{\partial u_0}{\partial \theta} + \frac{\partial v_0}{\partial r} - \frac{v_0}{r}, \frac{\partial u_1}{\partial r}, \frac{1}{r}\frac{\partial v_1}{\partial \theta} + \frac{u_1}{r}, \\ & \frac{1}{r}\frac{\partial u_1}{\partial \theta} + \frac{\partial v_1}{\partial r} - \frac{v_1}{r}, \frac{\partial u_1}{\partial r} + \frac{\partial^2 w_0}{\partial r^2}, \\ & \frac{1}{r}\left(u_1 + \frac{\partial w_0}{\partial r}\right), \frac{1}{r}\left(\frac{\partial u_1}{\partial \theta} + \frac{\partial^2 w_0}{\partial \theta \partial r}\right), \\ & \frac{1}{r}\left(\frac{\partial v_1}{\partial \theta} + \frac{1}{r}\frac{\partial^2 w_0}{\partial \theta^2}\right), \left(\frac{\partial v_1}{\partial r} + \frac{1}{r}\frac{\partial^2 w_0}{\partial r \partial \theta}\right) - \frac{1}{r}\left(v_1 + \frac{1}{r}\frac{\partial w_0}{\partial \theta}\right) \Bigg\}^T,\end{aligned} \tag{25}$$

the general transverse shear strain vector is defined as:

$$\{X\}_s = \left\{u_1 + \frac{\partial w_0}{\partial r}, v_1 + \frac{1}{r}\frac{\partial w_0}{\partial \theta}, u_1 + \frac{\partial w_0}{\partial r}, v_1 + \frac{1}{r}\frac{\partial w_0}{\partial \theta}\right\}^T. \tag{26}$$

The global stretching-bending material constants are defined as follows:

$$[D_b] = \begin{bmatrix} A & B & B^{1a} & B^{2a} \\ B & D & D^{1a} & D^{2a} \\ B^{1a} & D^{1a} & D^{1aa} & D^{12a} \\ B^{2a} & D^{2a} & D^{12a} & D^{2aa} \end{bmatrix}, \tag{27}$$

while the global transverse shear material constants are defined as

$$[D_s] = \begin{bmatrix} A_s & A_s^{1a} & A_s^{2a} \\ A_s^{1a} & A_s^{1aa} & A_s^{12a} \\ A_s^{2a} & A_s^{12a} & A_s^{2aa} \end{bmatrix}. \tag{28}$$

The resultant material constants appearing in (27) and (28) are evaluated as shown in Appendix B.

After substituting the displacement relation (11) into (25) and (26), we obtain the following relations:

$$\{X\}_b^L = [R]_b^L\{a\},$$
$$\{X\}_s = [R]_s\{a\}. \tag{29}$$

The unknown constants $\{a\}$ are related to the nodal displacement by substituting each nodal coordinate into displacement and rotations:

$$\{d_e\} = [B]\{a\}, \tag{30}$$

where $\{d_e\}$ represents the nodal d.o.f. and $[B]$ represents the transformation matrix. Thus the element stiffness matrix is obtained as follows. The linear bending-stretching stiffness matrix is

$$[K_e]_b^L = [B]^{-T} \int_{\theta_1}^{\theta_2} \int_{r_1}^{r_2} \left[R_b^L\right]^T [D_b] \left[R_b^L\right] r \, \mathrm{d}r \, \mathrm{d}\theta [B]^{-1}, \tag{31}$$

while the transverse shear stiffness matrix is

$$[K_e]_s = [B]^{-T} \int_{\theta_1}^{\theta_2} \int_{r_1}^{r_2} [R_s]^T [D_s][R_s] r \, \mathrm{d}r \, \mathrm{d}\theta [B]^{-1}. \tag{32}$$

The total element stiffness matrix is the superposition of (31) and (32):

$$[K_e] = [K_e]_b^L + [K_e]_s. \tag{33}$$

5. STRESS RECOVERY FROM THE FINITE ELEMENT SOLUTIONS

The governing equation of motion after assemblage is

$$\left[K^L\right]\{d\} = \{F\}. \tag{34}$$

The elemental displacements $\{d_e\}$ are obtained from $\{d\}$, which is the solution of (34), and are used in (29) to determine the mid-plane strains at any point. The

total in-plane strains at any point, distance z from the mid-plane are determined from the corresponding mid-plane strains as follows:

$$\begin{Bmatrix} e_r \\ e_\theta \\ \gamma_{r\theta} \end{Bmatrix}^{(k)} = \begin{bmatrix} 1 & 0 & 0 & z & 0 & 0 & z^{1a} & 0 & 0 & 0 & 0 \\ 0 & 1 & 0 & 0 & z & 0 & 0 & z^{1a} & 0 & z^{2a} & 0 \\ 0 & 0 & 1 & 0 & 0 & z & 0 & 0 & z^{1a} & 0 & z^{2a} \end{bmatrix} \{X_b\}^L. \tag{35}$$

The total transverse shear strains at any point, distance z from the mid-plane are calculated as

$$\begin{Bmatrix} \gamma_{rz} \\ \gamma_{\theta z} \end{Bmatrix}^{(k)} = \begin{bmatrix} 1 & 0 & z^{1aa} & 0 \\ 0 & 1 & 0 & z^{2aa} \end{bmatrix} \{X_s\}. \tag{36}$$

The strains calculated from (35) and (36) are used in (8) to obtain the in-plane normal stress and transverse shear stress distribution at various points through the thickness of the disk.

6. NUMERICAL EXAMPLES

The stress distributions for laminated annular disks are calculated for a concentrated transverse load at $r = 65$ mm, $\theta = 0°$. The finite element mesh consists of 192 elements and 224 nodes. The disk is clamped at the inner radius and the outer radius is assumed traction free. The problem configuration considered is the static centerpart of a head-rotating disk system in the information storage industry. The ZGEFA and ZGEDI routines from LINPACK are used to solve the linear system of equations. The geometric dimensions of the plate are as follows: $R_i = 32.5$ mm, $R_0 = 65$ mm.

The stresses are calculated at the integration point which is located at $r = 62.3$ mm, $\theta = 9.25°$. Higher-order zig-zag theory (SHZZ4 – present method) uses 3-point Gaussian quadrature for both stretching-bending and transverse shear terms as in the studies by Di Sciuva [10]. This 3-point scheme gives no shear locking effects and no zero energy modes for these three elements. To implement Mindlin–Reissner theory (SECT42) (Deoggyu Lee, [20]) we used a selective reduced integration scheme in which stretching-bending is integrated with 2-point Gaussian quadrature and transverse shear is integrated with 1-point Gaussian quadrature. Polar-orthotropy is specified by stating the angle β as marked in Fig. 2. The material constants used are as follows:

Material I($\beta = 0°$): $E_1 = 40E$, $E_2 = E$, $G_{12} = G_{31} = 0.6E$, $G_{23} = 0.5E$,
$\nu_{12} = 0.25$, $\rho = 1$;

Material II($\beta = 90°$): $E_1 = E$, $E_2 = 40E$, $G_{12} = G_{23} = 0.6E$, $G_{31} = 0.5E$,
$\nu_{12} = 0.25$, $\rho = 1$;

where $E = 1 \times 10^6$. Properties for material II are derived by transforming material I through 90°.

Figure 4 shows the mid-plane deformation of a polar-orthotropic symmetric 4 layer disk[I/II/II/I] for a concentrated load. In Fig. 5, the present method and Mindlin–Reissner predictions are of opposite signs for the in-plane normal stress at the interface 1 and interface 3. Further, the present method predicts a much higher in-plane normal stress at the top and bottom surfaces compared to the Mindlin–Reissner theory based predictions. Figure 6 shows that the present method satisfies the traction free boundary conditions and gives parabolic transverse shear stress distribution through the thickness while the Mindlin–Reissner based theory produces a constant transverse shear stress distribution in each layer and stress discontinuity at interface 1 and interface 3. In Fig. 7, the present method and the Mindlin–Reissner

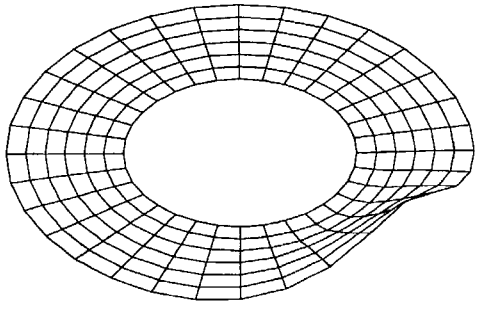

Figure 4. Mid-plane deformation of a polar-orthotropic symmetric 4 layer disk[I/II/II/I] for a concentrated transverse load.

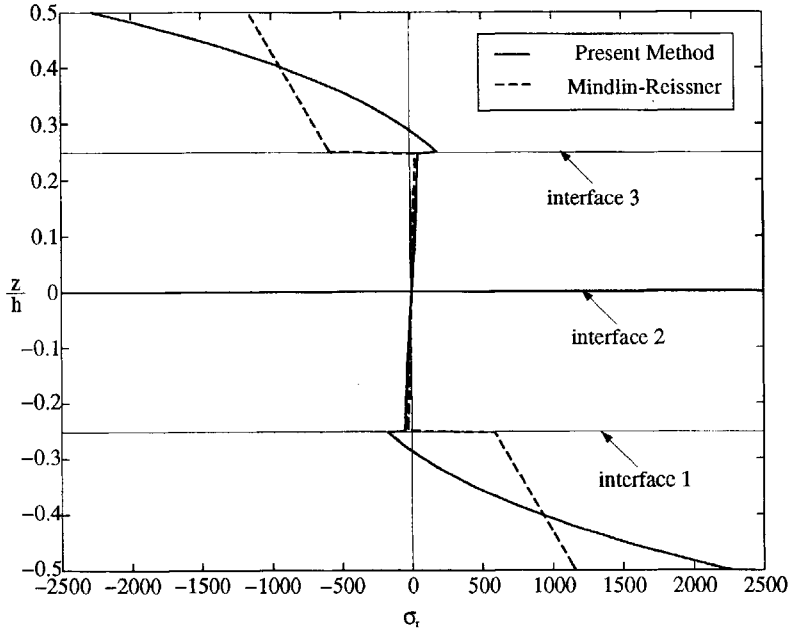

Figure 5. In-plane normal stress variation through the thickness of a polar-orthotropic symmetric 4 layer disk[I/II/II/I] for $R/h = 4$.

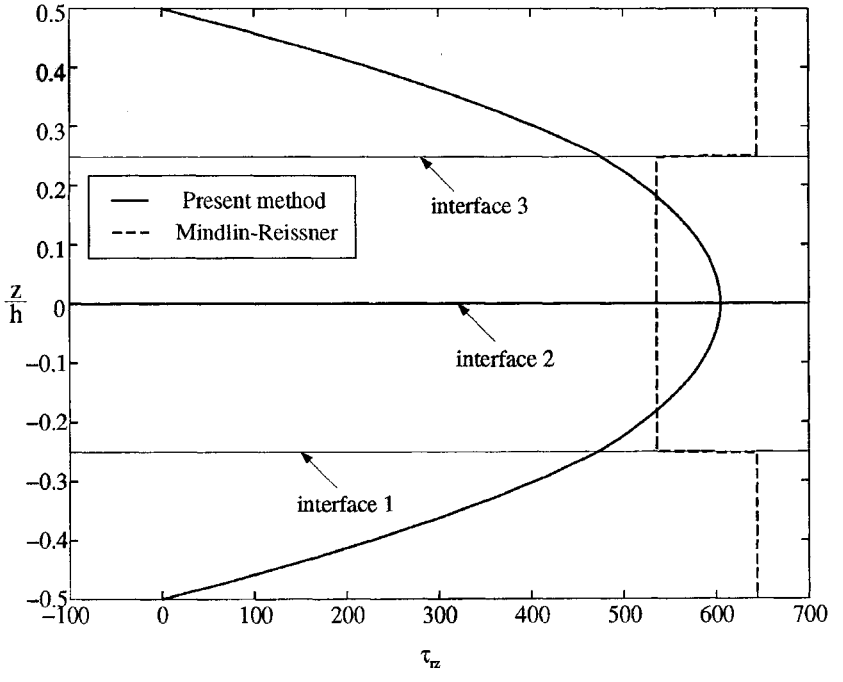

Figure 6. Transverse shear stress variation through the thickness of a polar-orthotropic symmetric 4 layer disk[I/II/II/I] for $R/h = 4$.

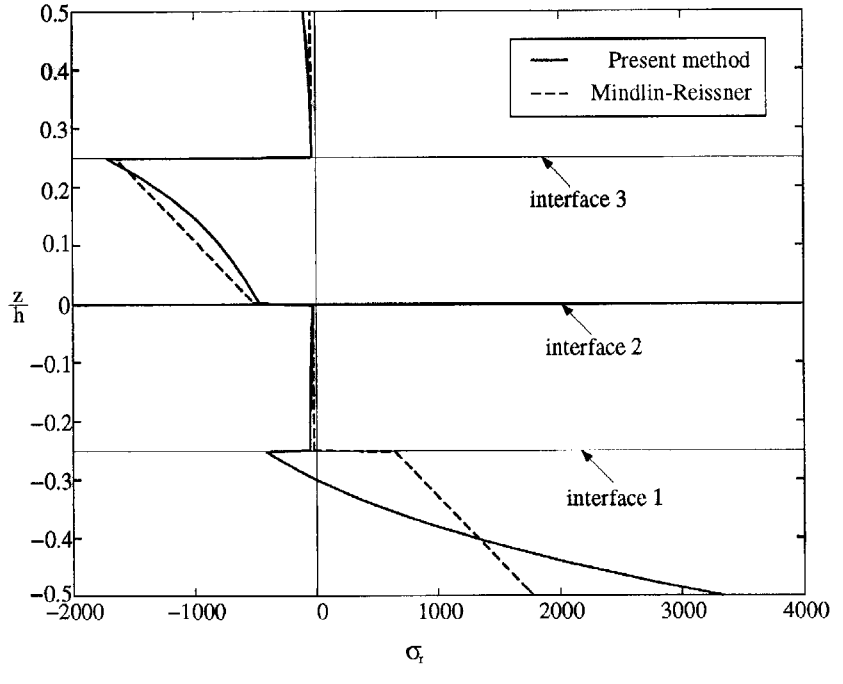

Figure 7. In-plane normal stress variation through the thickness of a polar-orthotropic antisymmetric 4 layer disk[I/II/I/II] for $R/h = 4$.

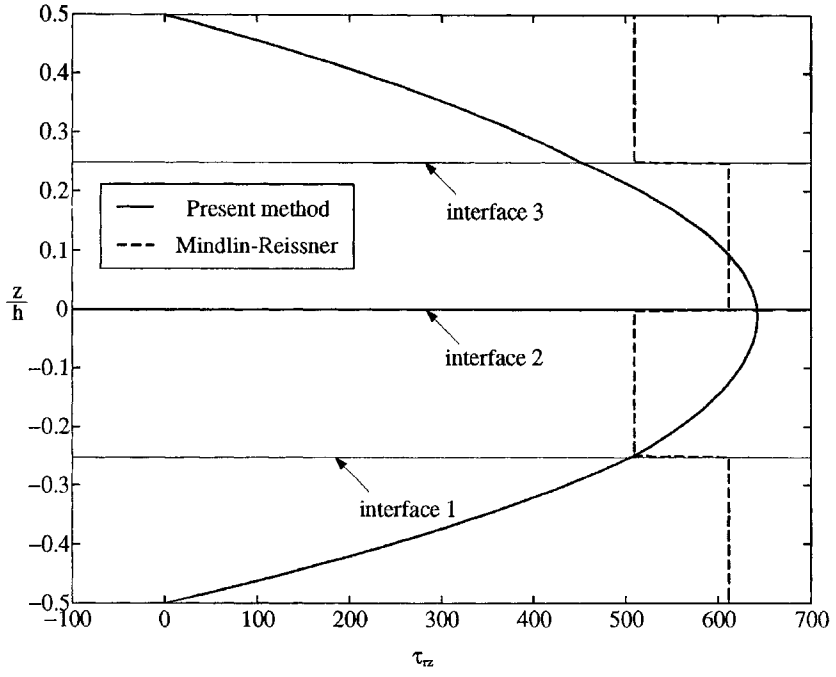

Figure 8. Transverse shear stress variation through the thickness of a polar-orthotropic anti-symmetric 4 layer disk[I/II/I/II] for $R/h = 4$.

predictions are of opposite signs for the in-plane normal stress at the interface 1 and the present method predicts much higher in-plane normal stress at the bottom surface. Figure 8 shows that the predictions of the present method satisfy traction free boundary conditions while Mindlin–Reissner theory based elements predict transverse shear stress discontinuities at interface 1, interface 2 and interface 3. As expected, the present method predictions for the symmetric lay-up[I/II/II/I] gives symmetric stress distribution with respect to the mid-plane, while the anti-symmetric lay-up[I/II/I/II] results in nonsymmetric stress distribution with respect to the mid-plane.

The results we have presented clearly show that the zig-zag theory is superior and accurate in predicting interlamina stress distribution for the problem considered. Thus, delamination initiation failure criteria, which are usually based on some function of the stress components becoming critical, will lead to erroneous results if a thickness averaged theory is used to compute the disk stress distribution. In the information storage industry, delamination failure of the disk renders it useless. Thus, the accurate prediction of failure initiation is crucial. While a discussion of the type of initiation criterion to be used is beyond the scope of this paper, it can be recommended quite safely that zig-zag theories are the more pertinent theories to use when computing stress distribution for use with failure criteria for layered materials.

7. CONCLUSION

In this paper we have presented a stress analysis of laminated annular disks subjected to a concentrated transverse load. A sector finite element (SHZZ4) incorporating higher order layer-wise zig-zag theory was developed and applied to the calculation of in-plane normal stress and transverse shear stress distribution through the thickness. These stress components are important in determining delamination failures in layered disks. SHZZ4 satisfies the shear stress continuity at the layer interfaces and traction free boundary conditions of the disk surfaces. It has a fixed number of degrees of freedom (7) regardless of the number of layers. It performed free of the shear locking effect. It was also devoid of hourglass modes due to the reduced integration of the stiffness matrix.

From the numerical results obtained in this work, SHZZ4 provides accurate transverse shear distribution through the thickness while the first order shear deformation theory (SECT42) gives constant transverse shear stress distribution in each layer and discontinuities in shear stress at the layer interfaces. Thus, SHZZ4 is highly recommended for use in predicting disk failure initiation with stress based criteria.

REFERENCES

1. Lo, K. H., Christensen, R. M. and Wu, E. M. A higher-order theory of plate deformation, Part 1: Homogeneous plates. *J. Appl. Mech.* **44**, 663–668 (Dec. 1977).
2. Putcha, N. S. and Reddy, J. N. A mixed shear flexible finite element for the analysis of laminated plates. *Computer Methods Appl. Mech. Engng* **44**, 213–227 (1984).
3. Reddy, J. N. and Phan, N. D. Stability and vibration of isotropic, orthotropic and laminated plates according to a higher-order shear deformation theory. *J. Sound Vib.* **98**, 157–170 (1985).
4. Mallikarjuna, A. and Kant, T. Free vibration of symmetrically laminated plates using a higher-order theory with finite element technique. *Int. J. Numer. Methods Eng.* **28**, 1875–1889 (1989).
5. Di Sciuva, M. Bending, vibration and buckling of simply supported thick multilayered orthotropic plates: an evaluation of a new displacement model. *J. Sound Vib.* **105**, 425–442 (1986).
6. Murakimi, H. Laminated composite plate theory with improved in-plane response. *J. Appl. Mech.* **53**, 661–666 (1986).
7. Di Sciuva, M. An improved shear-deformation theory for moderately thick multilayered anisotropic shells and plates. *J. Appl. Mech.* **54**, 589–596 (1987).
8. Wang, C. Y. and Yew, C. H. Impact damage in composite laminates. *Computer and Structures* **37**, 967–982 (1990).
9. Cho, M. and Parmerter, R. R. Efficient higher order composite plate theory for general lamination configuration. *AIAA Journal* **31**, 1299–1306 (1993).
10. Di Sciuva, M. A general quadrilateral multilayered plate element with continuous interlaminar stresses. *Computer and Structures* **47**, 91–105 (1993).
11. Averill, R. C. Static and dynamic response of moderately thick laminated beams with damage. *Compos. Engng* **4**, 381–395 (1994).
12. Averill, R. C. and Yip, Y. C. Development of simple, robust finite elements based on refined theories for thick laminated beams. *Computers and Structures* **59**, 529–546 (1996).
13. Reddy, J. N. A generalization of two-dimensional theories of laminated composite plates. *Communications Appl. Numer. Methods* **3**, 173–180 (1987).
14. Lu, X. and Liu, D. Interlayer shear slip theory for cross-ply laminates with nonrigid interfaces. *AIAA Journal* **30**, 1063–1073 (1992).

15. Nosier, A., Kapania, R. K. and Reddy, J. N. Free vibration analysis of laminated plates using a layer-wise theory. *AIAA Journal* **31**, 2335–2346 (1993).
16. Reddy, J. N. An evaluation of equivalent-single-layer and layer-wise theories of composite laminates. *Compos. Struct.* **25**, 21–35 (1993).
17. Cho, K. N., Bert, C. W. and Striz, A. G. Free vibrations of laminated rectangular plates analyzed by higher order individual layer theory. *J. Sound Vib.* **145**, 429–442 (1991).
18. Wu, C. P. and Hsu, C. S. A new local higher-order laminate theory. *Compos. Struct.* **25**, 439–448 (1993).
19. Thiel, G. H. and Miller, R. E. A finite element for the linear analysis of laminated circular plates. *Compos. Struct.* **27**, 339–355 (1994).
20. Lee, D. G. Vibration and stability analysis of a rotating multi-layer annular plate with a stationary load system. PhD dissertation, The University of Michigan (1996).
21. Whitney, J. M. Shear correction factors for orthotropic laminates under static load. *Trans. ASME* 302–304 (March 1973).
22. Washizu, K. *Variational Methods in Elasticity and Plasticity*, 3rd edn. Pergamon (1982).
23. Fung, Y. C. *Foundations of Solid Mechanics*. Prentice Hall (1965).
24. Bathe, K. J. *Finite Element Procedures in Engineering Analysis*. Prentice Hall (1982).
25. Jones, R. M. *Mechanics of Composite Materials*. McGraw-Hill (1975).

APPENDIX A: THE COEFFICIENTS IN THE REFINED HIGHER ORDER ZIG-ZAG DISPLACEMENT FIELD

The coefficients in the refined higher order zig-zag displacement field are defined as follows:

$$\tilde{a}_i^k = \left\{ \frac{\hat{a}_i^k}{1 + \sum_{j=1}^{m} \hat{a}_j^k} \right\}, \tag{A1}$$

$$\tilde{b}_i^k = \left\{ \hat{b}_i^k - \tilde{a}_i^k \sum_{j=1}^{m} \hat{b}_j^k \right\}, \tag{A2}$$

$$\tilde{c}_i^k = \left\{ \hat{c}_i^k - \tilde{a}_i^k \sum_{j=1}^{m} \hat{c}_j^k \right\}, \tag{A3}$$

$$\hat{a}_i^k = \left(\frac{G_{k3}^{(i)}}{G_{k3}^{(i+1)}} - 1 \right) \left(1 + \sum_{j=1}^{i-1} \hat{a}_j^k \right), \tag{A4}$$

$$\hat{b}_i^k = \left(\frac{G_{k3}^{(i)}}{G_{k3}^{(i+1)}} - 1 \right) \left(2z_i + \sum_{j=1}^{i-1} \hat{b}_j^k \right), \tag{A5}$$

$$\hat{c}_i^k = \left(\frac{G_{k3}^{(i)}}{G_{k3}^{(i+1)}} - 1 \right) \left(3z_i^2 + \sum_{j=1}^{i-1} \hat{c}_j^k \right), \tag{A6}$$

(note that $k = 1, 2$ and $1 = r$, $2 = \theta$),

$$a_i^k = \tilde{a}_i^k + \tilde{b}_i^k \beta_k + \tilde{c}_i^k \kappa_k, \tag{A7}$$

$$\beta_k = \frac{1}{\Delta_k}\left[\left(3z_0^2 - \sum_{i=1}^{m}\tilde{c}_i^k\right)\left(1 + \sum_{j=m+1}^{N-1}\tilde{a}_j^k\right) - \left(3z_N^2 + \sum_{i=m+1}^{N-1}\tilde{c}_i^k\right)\left(1 - \sum_{j=1}^{m}\tilde{a}_j^k\right)\right]. \tag{A8}$$

$$\kappa_k = -\frac{1}{\Delta_k}\left[\left(2z_0 - \sum_{i=1}^{m}\tilde{b}_i^k\right)\left(1 + \sum_{j=m+1}^{N-1}\tilde{a}_j^k\right) - \left(2z_N + \sum_{i=m+1}^{N-1}\tilde{b}_i^k\right)\left(1 - \sum_{j=1}^{m}\tilde{a}_j^k\right)\right], \tag{A9}$$

$$\Delta_k = \left(2z_0 - \sum_{i=1}^{m}\tilde{b}_i^k\right)\left(3z_N^2 + \sum_{j=m+1}^{N-1}\tilde{c}_j^k\right) - \left(2z_N + \sum_{i=m+1}^{N-1}\tilde{b}_i^k\right)\left(3z_N^2 - \sum_{j=1}^{m}\tilde{c}_j^k\right). \tag{A10}$$

APPENDIX B: THE RESULTANT MATERIAL CONSTANTS

Using the constitutive relations, we obtain the following material constants:

$$\left[A_{ij} \quad B_{ij} \quad D_{ij}\right] = \sum_{k=1}^{N}\int_{z_{k-1}}^{z_k}\left[1 \quad z \quad z^2\right]C_{ij}^{(k)}\,\mathrm{d}z, \tag{B1}$$

where $i, j = 1, 2, 3$;

$$\left[B_{ij}^{1a} \quad B_{ij}^{1a} \quad D_{ij}^{1aa}\right] = \sum_{k=1}^{N}\int_{z_{k-1}}^{z_k}\left[z^{1a} \quad zz^{1a} \quad \left(z^{1a}\right)^2\right]C_{ij}^{(k)}\,\mathrm{d}z, \tag{B2}$$

where $i, j = 1, 2, 3$;

$$\left[B_{ij}^{2a} \quad D_{ij}^{2a} \quad D_{ij}^{12a}\right] = \sum_{k=1}^{N}\int_{z_{k-1}}^{z_k}\left[z^{2a} \quad zz^{2a} \quad z^{1a}z^{2a}\right]C_{ij}^{(k)}\,\mathrm{d}z, \tag{B3}$$

where $i = 1, 2, 3$ and $j = 2, 3$;

$$\left[D_{ij}^{2aa}\right] = \sum_{k=1}^{N}\int_{z_{k-1}}^{z_k}\left[\left(z^{2a}\right)^2\right]C_{ij}^{(k)}\,\mathrm{d}z, \tag{B4}$$

where $i, j = 2, 3$;

$$\left[A_{ij}^{s}\right] = \sum_{k=1}^{N}\int_{z_{k-1}}^{z_k} C_{ij}^{(k)}\,\mathrm{d}z, \tag{B5}$$

where $i, j = 4, 5$;

$$\left[A_{ij}^{s1a}\right] = \sum_{k=1}^{N}\int_{z_{k-1}}^{z_k}\left[z^{1aa}\right]C_{ij}^{(k)}\,\mathrm{d}z, \tag{B6}$$

where $i = 4$ and $j = 4, 5$;

$$\left[A_{ij}^{s2a}\right] = \sum_{k=1}^{N}\int_{z_{k-1}}^{z_k}\left[z^{2aa}\right]C_{ij}^{(k)}\,\mathrm{d}z, \tag{B7}$$

where $i = 4, 5$ and $j = 5$;

$$\left[A_{ij}^{s1aa}\right] = \sum_{k=1}^{N}\int_{z_{k-1}}^{z_k}\left[\left(z^{1aa}\right)^2\right]C_{ij}^{(k)}\,\mathrm{d}z, \tag{B8}$$